Bulletin of the Seismological Society of America, Vol. 103, No. 1, pp. 211–222, February 2013, doi: 10.1785/0120120161

Stable Stress-Drop Measurements and their Variability: Implications for Ground-Motion Prediction

by Annemarie S. Baltay, Thomas C. Hanks, and Gregory C. Beroza

Abstract We estimate the a_{rms}-stress drop, $\Delta\sigma$-a_{rms}, (Hanks, 1979) using acceleration time records of 59 earthquakes from two earthquake sequences in eastern Honshu, Japan. These acceleration-based static stress drops compare well to stress drops calculated for the same events by Baltay *et al.* (2011) using an empirical Green's function (eGf) approach. This agreement supports the assumption that earthquake acceleration time histories in the bandwidth between the corner frequency and a maximum observed frequency can be considered white, Gaussian, noise. Although the $\Delta\sigma$-a_{rms} is computationally simpler than the eGf-based f_c-M_0-stress drop, and is used as the "stress parameter" to describe the earthquake source in ground-motion prediction equations, we find that it only compares well to the $\Delta\sigma$-eGf at source-station distances of ~20 km or less because there is no consideration of whole-path anelastic attenuation or scattering. In these circumstances, the correlation between the $\Delta\sigma$-eGf and $\Delta\sigma$-a_{rms} is strong. Events with high and low stress drops obtained through the eGf method have similarly high and low $\Delta\sigma$-a_{rms}. We find that the inter-event standard deviation of stress drop, for the population of earthquakes considered, is similar for both methods, 0.40 for the $\Delta\sigma$-eGf method and 0.42 for the $\Delta\sigma$-a_{rms}, in $\log_{10}$ units, provided we apply the ~20 km distance restriction to $\Delta\sigma$-a_{rms}. This indicates that the observed variability is inherent to the source, rather than attributable to uncertainties in stress-drop estimates.

Online Material: Earthquake catalog including additional source parameters.

Introduction

While the earthquake engineering community has recognized the affinity of earthquake ground accelerations to white noise for more than half a century (e.g., Housner, 1947; Bycroft, 1960), earthquake scientists came to appreciate this association only with the advent and rapid advances of seismic source theory in the 1970s. The ω^{-2} model for the high-frequency spectral decay of far-field displacement spectra of the Aki (1967) and Brune (1970) source models was first interpreted as a phase-coherent delta-function in ground acceleration. Hanks (1979) noted that a finite-duration, phase-incoherent model might be a better interpretation, given the characteristics of the few close-in strong-motion accelerograms then existing.

Hanks (1979) related earthquake stress drop to the root mean square (rms) value of acceleration time histories beginning at the *S*-wave arrival, for close distances, by utilizing Parseval's theorem and several operational assumptions to find

$$\Delta\sigma_{a\mathrm{rms}} = a_{\mathrm{rms}} \frac{106\rho R}{2R_{\theta\phi}(2\pi)^2} \sqrt{\frac{f_c}{f_{\mathrm{max}}}}, \qquad (1)$$

where f_c is the earthquake corner frequency, f_{max} is the observational upper limit of the recording, $R_{\theta\phi}$ is the shear-wave radiation pattern, and R is the source-site distance. McGuire and Hanks (1980) explored several aspects of a_{rms} and the associated stress drop, $\Delta\sigma$-a_{rms} (equation 1), for the large set of strong ground-motion data available from the M 6.6 1971 San Fernando earthquake, also noting a strong correlation between a_{rms} and peak ground acceleration (PGA). Hanks and McGuire (1981) extended the analysis of $\Delta\sigma$-a_{rms} for 15 other California earthquakes. The assumption that ground accelerations in the *S*-wave arrival window are finite-duration, bandlimited, white noise combined with elementary random-vibration theory led to a simple relation between a_{rms} and PGA.

Hanks and McGuire (1981) also found that the $\Delta\sigma$-a_{rms} of the 16 considered earthquakes showed relatively little variability nor dependence on magnitude, all close to 10 MPa, with standard deviation of 0.15 ($\log_{10}$ units; 95% confidence interval of 0.3 in Hanks and McGuire [1981]). Stress drops determined from the more commonly applied method of

using corner frequency, f_c, and long period spectral level (proportional to moment, M_0) (Brune, 1970),

$$\Delta\sigma_{f_c-M_0} = \frac{7M_0}{16}\left(\frac{2\pi f_c}{2.34\beta}\right)^3, \quad (2)$$

show considerably greater variability, with standard deviations between 0.3 and 0.7 ($\log_{10}$ units; e.g., Thatcher and Hanks, 1973; Hanks, 1977; Shearer *et al.*, 2006; Allmann and Shearer, 2009). In both formulations, the stress drops are scaled to the Brune (1970) source spectrum, so in principle they should be the same.

The $\Delta\sigma$-$a_{\rm rms}$ as proposed by Hanks (1979) measures the high-frequency part of the source spectrum and has only a weak dependence on the corner frequency (equation 1); whereas, the typical formulation for stress drop (equation 2) depends on the cube of the corner frequency. For this reason, $\Delta\sigma$-$a_{\rm rms}$ measurements are much less susceptible to noise or errors in corner frequency, for any single event, than $\Delta\sigma$-f_c-M_0. Hanks and McGuire (1981) surmised that the observed decreased variability in the $\Delta\sigma$-$a_{\rm rms}$, as compared to $\Delta\sigma$-f_c-M_0, was due to the reduced dependence on propagated errors from the corner frequency estimates. Because $\Delta\sigma$-$a_{\rm rms}$ is derived from the high-frequency end of the spectrum, however, its estimation as formulated by Hanks (1979) should only be valid at close distances where corrections for anelastic attenuation are small, and can be approximated by limiting the bandwidth of interpreted signal. Since the work of Hanks and McGuire (1981), little effort has been made to compare and contrast $\Delta\sigma$-$a_{\rm rms}$ and $\Delta\sigma$-f_c-M_0 for the same earthquakes, perhaps because the $\Delta\sigma$-$a_{\rm rms}$ was so quickly adopted for use in earthquake ground-motion prediction.

Boore (1983) developed the "stochastic method" of generating earthquake acceleration spectra and time series by adapting the ideas behind Hanks and McGuire (1981), that ground accelerations excited by earthquakes are bandlimited, finite-duration white Gaussian noise. $\Delta\sigma$-$a_{\rm rms}$ is used as the "stress parameter" in the stochastic method as the main control for the level of high-frequency strong ground motion. Through improvements in the random vibration part of the Hanks and McGuire (1981) model, Boore (1983) showed that these assumptions generate realistic spectral series, for both acceleration and velocity, as well as response spectra, PGA, and peak ground velocity (PGV) over a range of distances, and, for large earthquakes of $5.0 \le M_{\rm w} \le 7.7$. The ground-motion prediction community generally considers the stress parameter ($\Delta\sigma$-$a_{\rm rms}$) to be independent of moment, although its median value and standard deviation is observed to be dependent on tectonic setting. $\Delta\sigma$-$a_{\rm rms}$ has become increasingly important for calibrating ground-motion prediction in data-poor regions as a key input parameter to the stochastic method of simulating ground motion (e.g., Atkinson and Boore, 2006). Other studies compared strong-motion observations to stochastic simulations to obtain the best-fitting stress parameter by accounting for path effects and variable geometrical spreading parameters for earthquakes in Greece and eastern North America (e.g., Margaris and Boore, 1998; Boore *et al.*, 2010; Boore, 2012). Beyond its application to ground-motion prediction, however, $\Delta\sigma$-$a_{\rm rms}$ is not widely recognized in the seismology community, and has not been used recently as a source parameter in earthquake physics studies. None of the previous work rigorously compares the formulation and estimation of $\Delta\sigma$-$a_{\rm rms}$ with the $\Delta\sigma$-f_c-M_0 on the same earthquake data.

Revisiting $\Delta\sigma$-$a_{\rm rms}$ is of interest for several reasons. At the time of the original study, $\Delta\sigma$-f_c-M_0 was often estimated using crude corrections, if any at all, for attenuation or path effects. Because stress-drop variability is often driven by corner frequency uncertainty, the $\Delta\sigma$-$a_{\rm rms}$ yielded much less variability. In recent work, Baltay *et al.* (2011) use a robust empirical Green's function (eGf) technique to remove path effects to estimate $\Delta\sigma$-f_c-M_0 from corner frequency estimates. By comparing the $\Delta\sigma$-$a_{\rm rms}$ to the eGf-based $\Delta\sigma$-f_c-M_0 (hereafter $\Delta\sigma$-eGf) we can better assess the viability of both methods and the uncertainties associated with each. Second, $a_{\rm rms}$ is very simple to measure, and is only slightly dependent on the corner frequency, which may be known or roughly estimated. For that reason, each record can be analyzed independently, without being dependent on the existence of an eGf event. The algorithm for $\Delta\sigma$-$a_{\rm rms}$ is computationally simple with fewer assumptions, and has potential to be developed for use in real time. In fact, rms-acceleration is one of the simplest measurements that can be made on a single recording. Finally, revisiting $\Delta\sigma$-$a_{\rm rms}$ with recent earthquake data from a seismological perspective may renew its interest as an earthquake source parameter.

In this study, we test the relationships developed by Hanks (1979) using a much larger and better data set of 59 earthquakes, spanning a wide range of magnitudes and source-site distances (Fig. 1). We measure the $a_{\rm rms}$ of two mainshock–aftershock sequences from KiK-net accelerograms in eastern Honshu, Japan, that have been previously

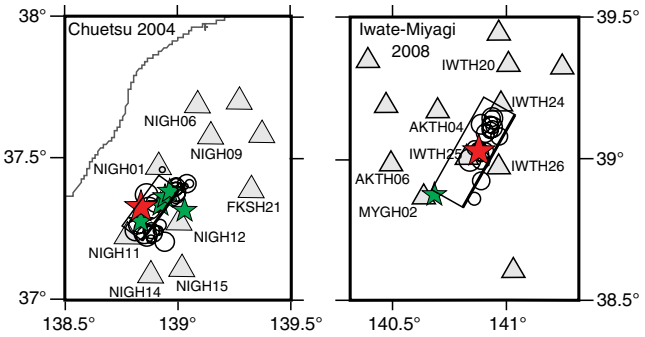

Figure 1. Map showing mainshock, large star; largest aftershocks, smaller stars; all other aftershocks, open circles; and location of stations which are within distances of less than 30 km. Fault plane from Hikima and Koketsu (2005) for Chuetsu 2004, and Suzuki *et al.* (2010) for Iwate-Miyagi 2008. The color version of this figure is available only in the electronic edition.

studied by Baltay *et al.* (2011), and compare $\Delta\sigma$-$a_{\rm rms}$ to $\Delta\sigma$-eGf.

We find that $\Delta\sigma$-$a_{\rm rms}$ compares well to $\Delta\sigma$-eGf of Baltay *et al.* (2011) and can be easily computed from $a_{\rm rms}$ measurements, which supports the analyses performed by Hanks (1979), McGuire and Hanks (1980), and Hanks and McGuire (1981). While the algorithm behind the $\Delta\sigma$-$a_{\rm rms}$ is straightforward, the $a_{\rm rms}$ approach for stress drop described here does not consider frequency-dependent anelastic attenuation, only a simple $1/R$ geometrical spreading correction, and suffers from loss of amplitude at farther stations. For small events, $\Delta\sigma$-$a_{\rm rms}$ for stations with distance less than 20 km compares well to the $\Delta\sigma$-eGf; at greater distances, $\Delta\sigma$-$a_{\rm rms}$ is less than $\Delta\sigma$-eGf. Although earlier studies of Hanks (1979) and McGuire and Hanks (1980) find that the $a_{\rm rms}$ approach for stress drop was much less variable, our population of $\Delta\sigma$-eGf estimates (with standard deviation 0.40 $\log_{10}$ units) shows a variability comparable to $\Delta\sigma$-$a_{\rm rms}$ (standard deviation = 0.42 $\log_{10}$ units). The overall distribution of event stress drops is similar between methods, implying that the eGf method is an improvement over methods that consider only elementary path corrections, such as Thatcher and Hanks (1973) and Hanks (1977). When considering corner frequency as the only source of uncertainty, the uncertainty in $\Delta\sigma$-$a_{\rm rms}$ for any single earthquake is smaller than the uncertainty of $\Delta\sigma$-eGf; however, other sources of uncertainty certainly exist, such as other source parameters (moment, for one), assumptions about the source model, and the iterative relative deconvolution scheme employed in the eGf method of Baltay *et al.* (2011).

We also estimate PGA from $a_{\rm rms}$ and compare the data to the theoretical PGA using the previously established relationship of Hanks and McGuire (1981), together with an input stress-drop distribution from Baltay *et al.* (2011). We confirm that PGA is predictable from $a_{\rm rms}$, and that data match the theoretical relations of Hanks and McGuire (1981) at close distances for all magnitudes, and for the larger earthquakes, for which the amplitude is negligibly affected by attenuation. The ability to predict PGA, given only an *a priori* stress-drop distribution and knowledge of the source duration, strongly supports the original observation that acceleration time histories can be treated as Gaussian white noise above the corner frequency. While earthquake ground-motion modelers have extensively studied PGA prediction, the simple relationships here for PGA elucidate key source dependencies in terms more interesting to the general seismology community.

While we find $\Delta\sigma$-$a_{\rm rms}$ formulation (equation 1) to be valid for estimating stress drops at short source-station distances ($R \leq 20$ km), the eGf f_c-M_0 method is capable of using data from stations at greater distances. The computational simplicity of the $\Delta\sigma$-$a_{\rm rms}$ retains its appeal for some applications, such as real-time source assessment, source parameter determination in data-sparse situations, and for use in engineering ground-motion equations. Finally, our larger data set allows us to quantify the aleatory variability of stress drop. Measured variability (standard deviation) is similar for the two approaches, which supports the notion that inter-event variability in stress drop is largely intrinsic to the earthquake source, and is not simply a measurement bias due to errors in corner frequency.

Empirical Green's Function Stress Drops

Baltay *et al.* (2011) used an empirical eGf coda-based method to determine source parameters, including $\Delta\sigma$-f_c-M_0, for four crustal earthquake sequences in Honshu, Japan. They modeled source spectra stacked from broadband Hi-Net velocity recordings at many stations using a Brune ω^{-2} spectrum (Brune, 1970) to fit a corner frequency. The Brune stress drop is estimated from the corner frequency as in Baltay *et al.* (2011), using a shear-wave velocity, $\beta = 3600$ m/s, and density, $\rho = 2800$ kg/m^3 (equation 2).

Of the data analyzed by Baltay *et al.* (2011), two sequences will be considered in this study: the 2008 $M_{\rm w}$ 6.9 Iwate-Miyagi Nairiku mainshock and 26 aftershocks; and the 2004 $M_{\rm w}$ 6.6 Chuetsu (mid-Niigata) earthquake and 31 aftershocks (Fig. 1). The other two sequences studied by Baltay *et al.* (2011), Chuetsu-Oki 2007 and the off-Kamaishi repeating events, are not considered here as they are both offshore, and hence the source-station distances are too large for $\Delta\sigma$-$a_{\rm rms}$ estimation. In aggregate for all 59 events, $\log_{10}$ $\Delta\sigma$-eGf follows a normal distribution with an equivalent median stress drop of 5.0 MPa and standard deviation of 0.4 ($\log_{10}$ units; see Fig. 4 and Ⓔ Table S1 from Baltay *et al.* [2011]; data used here with permission from American Geophysical Union).

$a_{\rm rms}$ Stress Drop

The ω^{-2} model (Aki, 1967; Brune, 1970) for earthquake acceleration source spectra is flat for frequencies $f > f_c$, which is consistent with white noise if the phase can be considered random. Hanks and McGuire (1981) assumed that acceleration spectrum results from random white noise, consistent with a far-field ω^{-2} model, generated by a time series for the finite duration of the *S*-wave arrival window, from $t = 0$ (*S*-wave arrival) to $t = T_d$, the duration of faulting. Based on a demonstration that acceleration time histories were Gaussian in the finite-duration window, they posited that high-frequency acceleration is finite-duration, band-limited, white Gaussian noise, an assumption that has been central to ground-motion prediction ever since. They also showed that the relationship between $a_{\rm rms}$ and PGA was predictable using random vibration theory, providing a stringent test on the assumption that the acceleration time series is in fact equivalent to Gaussian white noise. They observed, however, a frequency limit, $f_{\rm max}$, on the acceleration spectrum, above which the spectrum decays rapidly.

The cause and implication of $f_{\rm max}$ was explored by several authors, debating whether it was a local site effect, or a condition of the earthquake source (e.g., Archuleta *et al.*, 1982; Hanks, 1982; Papageorgiou and Aki, 1983).

Ultimately, it was concluded that $f_{\max}$ is a property of local site or instrument conditions, related to the near-site attenuation parameter κ which describes the rapid decay of high-frequency acceleration spectra of the form $\exp(-\pi\kappa f)$ (Anderson and Hough, 1984; Boore, 2003). $f_{\max}$ can be related to κ as $f_{\max} \sim (\pi\kappa)^{-1}$; however for small magnitudes this becomes a poor approximation (Anderson, 1986). For our study, $f_{\max}$ is important because it places an upper frequency limit, below which acceleration can be considered to be white noise. The usage of $f_{\max}$ here is consistent with that of Hanks (1979), Hanks and McGuire (1981), and Hanks (1982), defined such that the maximum spectral level between f_c and $f_{\max}$ is constant and the integral of such implies an rms value equal to that of the actual spectrum. It is perhaps more consistent with the concept of f_{95} introduced by Anderson (1986) as a quantitative equivalent to $f_{\max}$ rather than the $(\pi\kappa)^{-1}$ approximation. We also note that this use of $f_{\max}$ considers only the frequency value above which the spectra are no longer considered white Gaussian noise, and does not imply a functional model of the high-frequency decay as posed by Anderson and Hough (1984).

The rms value of an acceleration time history can be related to stress drop (equation 3), corner frequency, and $f_{\max}$, as in equation (1), as derived by Hanks (1979) and recapitulated in Appendix A. In this study, we take R as the catalog hypocentral distance. For the larger earthquakes, this distance may not be the most applicable, but it is the simplest for our case.

The $\Delta\sigma$-$a_{\rm rms}$ varies as $f_c^{1/2}$, whereas the expression for $\Delta\sigma$-f_c-M_0 varies as f_c^3 (equation 2). Estimates of corner frequency are often highly variable and may be strongly dependent on the method employed or assumptions made (e.g., Sonly and Abercrombie, 2006; Kane *et al.*, 2011). Inadequate site attenuation corrections can also affect the measured corner frequency. For events up to M 3 with high attenuation, $f_{\max}$ becomes the observable corner frequency resulting in an underestimation of corner frequency and stress drop; for events as large as M 4.5, with moderate values of $\kappa = 0.05$, the apparent corner frequency varies from the true corner frequency by a factor of 2 (Anderson, 1986). Even for larger events, $\sim M$ 5, stress drop can be underestimated by more than a factor of 2, because the log error in $\Delta\sigma$-f_c-M_0 is thrice that of the log error in f_c. Based on corner frequency dependence alone, the $\Delta\sigma$-$a_{\rm rms}$ should be much less variable than the $\Delta\sigma$-f_c-M_0; however, we find that the eGf method reduces the uncertainties to the point that the $\Delta\sigma$-$a_{\rm rms}$ and $\Delta\sigma$-eGf of a population of events compare closely.

In the following analysis, we estimate $\Delta\sigma$-$a_{\rm rms}$ by measuring the rms-acceleration, $a_{\rm rms}$, for events with *a priori* corner frequencies from previous studies, for which R, the hypocentral distance, is known, $f_{\max}$ is estimated, and ρ is assumed to be constant. We use acceleration data for 52 earthquakes from two mainshock-aftershock sequences in eastern Honshu, Japan, recorded at KiK-net borehole and surface stations (Fig. 2), consistent with the data from the eGf study. Because the ground motions are larger on the horizontal components, and the $a_{\rm rms}$ formulation in equation (1) accounts for equal partitioning, records are vectorally-averaged horizontal acceleration. For both earthquake

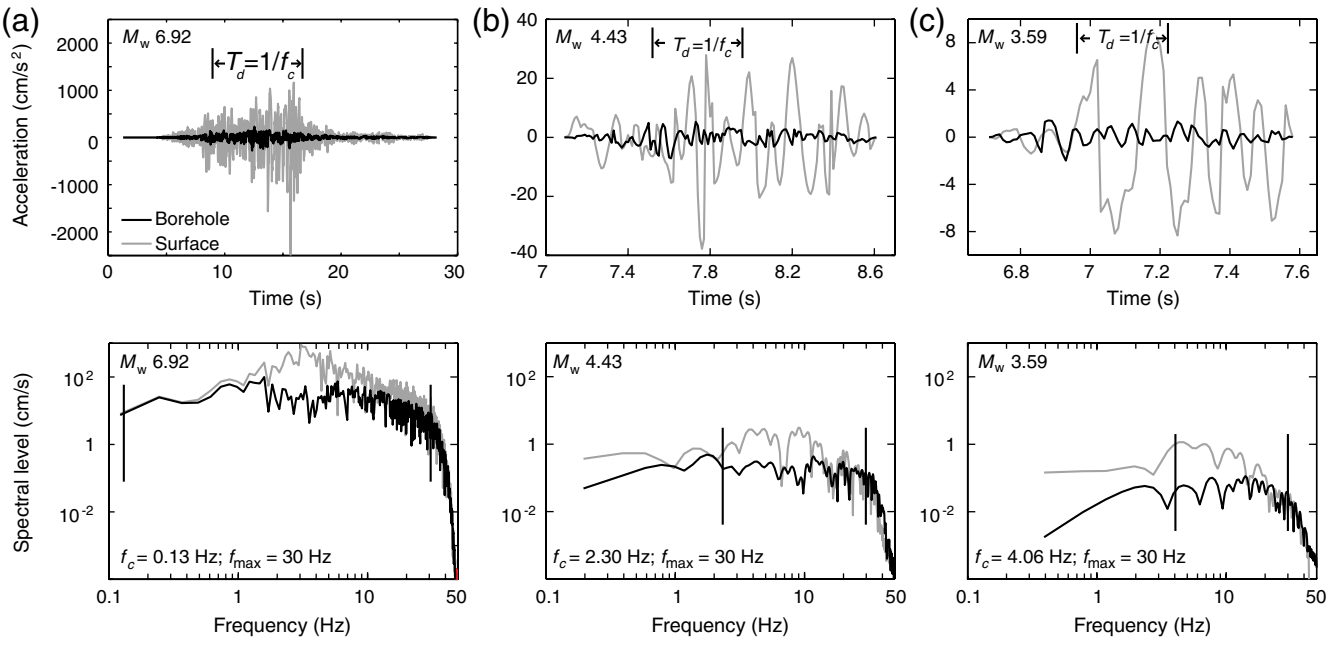

Figure 2. Time series (top row) and spectra (bottom row) for three events from the Iwate-Miyagi 2008 sequence, recorded at KiK-net station AKTH04, showing both borehole and surface recordings. Note different time and amplitude scales on time-series. In each case, we show the corner frequency, f_c, set *a priori* from Baltay *et al.* (2011) and $f_{\max} = 30$ Hz, (top row) and associated faulting duration, $T_d = 1/f_c$ used in the rms-acceleration calculation, as calculated from the given f_c.

sequences considered, the corner frequency, f_c, and seismic moment, M_0, were previously determined by Baltay *et al.* (2011).

We measure the rms acceleration, a_{rms}, of the time series from the horizontally averaged acceleration data, a very simple measurement on a single recording (Fig. 2). We choose a window of duration $T_d = 1/f_c$, with f_c set *a priori* from Baltay *et al.* (2011). The starting point of the window for each event-station pair is found by maximizing the rms acceleration within the window of both the borehole and surface data at the same time, so that we are capturing the greatest amount of signal in the measurement. In practice, the apparent duration will only be equal to the true source duration at stations perpendicular to the fault trace. At other stations, the recorded duration will be longer or shorter due to source finiteness; however, rms measurement is not strongly dependent on the duration of the window used.

By visually analyzing all the data, we find that the acceleration spectra recorded at distances $R \leq 30$ km are relatively flat up to 30 Hz; at higher frequencies the spectra decay rapidly (Fig. 3). Equation (1) for $\Delta\sigma$-a_{rms}, considered here, assumes that $f_{\max}$, as defined by Hanks (1982), is the frequency below which the spectrum is flat, Gaussian white noise, so that the integral given in equation (A2) can be approximated as a constant from f_c to $f_{\max}$. Hence, it is important to use an observed $f_{\max}$ with this purpose in mind, rather than adopting $f_{\max}$ or κ values from previous work. Studies of κ for KiK-net sites in Japan find a difference between the surface and borehole records, with typical values of 0.015 s for borehole and 0.029 s for surface (Oth *et al.*, 2011). However, we note that there is a strong trade-off between κ, or $f_{\max}$, and surface amplification, which can be seen in Figure 3. The surface spectra (top three traces) start to decay at a lower frequency than the borehole records (bottom three traces), which could be interpreted as a smaller $f_{\max}$, consistent with a larger surface κ. However, we interpret this effect to be due to surface amplification, which is evident in the M_{w} 4.4 event in Figure 2. The surface spectra are amplified between ~2 and ~10 Hz; above ~10 Hz they closely match the borehole spectra; and both start to rapidly decay at $f_{\max} = 30$ Hz. Therefore, we use a constant $f_{\max} = 30$ Hz in this study for both borehole and surface data, at all stations. Using the borehole value for κ of 0.015 s (Oth *et al.*, 2011) we find that the observed $f_{\max}$ here of 30 Hz can roughly be approximated as $f_{\max} \sim 3/(2\pi\kappa)$. Because $\Delta\sigma$-a_{rms} is dependent on $f_{\max}^{-1/2}$, using an $f_{\max}$ of 20 Hz or 50 Hz would result in $\Delta\sigma$-a_{rms} error of ~22%, while $f_{\max} = 10$ Hz would yield $\Delta\sigma$-a_{rms} different by ~73%.

$\Delta\sigma$-a_{rms} is thus determined from equation (1) with $\rho = 2800$ kg/m^3, $\beta = 3600$ m/s, $f_{\max} = 30$ Hz, and the previously determined corner frequencies. Figure 4a shows $\Delta\sigma$-a_{rms} for the Iwate-Miyagi mainshock and two aftershocks of M_{w} 4.4 and M_{w} 3.6. We find the surface $\Delta\sigma$-a_{rms} to be, on average, about a factor of 4 larger than those determined from borehole measurements. Amplification in the upper ~100 m between the borehole and surface stations and the complex interaction of direct phases and free surface reflected phases accounts for the difference between the borehole and surface estimates. Without careful consideration of these complex effects, we cannot say exactly what they are, but we attribute about a factor of two to each of free-surface amplification and material/impedance contrast between the borehole and surface station (e.g., Boore *et al.*, 2011; D. Boore, personal comm., 2012). The factor of two difference in κ between the borehole and surface stations (Oth *et al.*, 2011) would account for an increase in surface $\Delta\sigma$-a_{rms} of ~1.4. Because the $\Delta\sigma$-a_{rms} was originally formulated for, and meant to be applied to, surface measurements, in the analysis that follows we only compare the surface measurements to the $\Delta\sigma$-eGf.

For the mainshock, the $\Delta\sigma$-a_{rms} is stable at all source-station distances and decays slightly at $R > 50$ km (Fig. 4). The M_{w} 4.4 aftershock, however, shows stress drop decaying at stations farther than ~20 km, and the M_{w} 3.6 aftershock shows even stronger decay of estimated stress-drop values with distance. Because smaller events have higher corner frequencies, and hence smaller bandwidth between f_c and $f_{\max}$ as compared to larger events (Fig. 2, bottom row), their

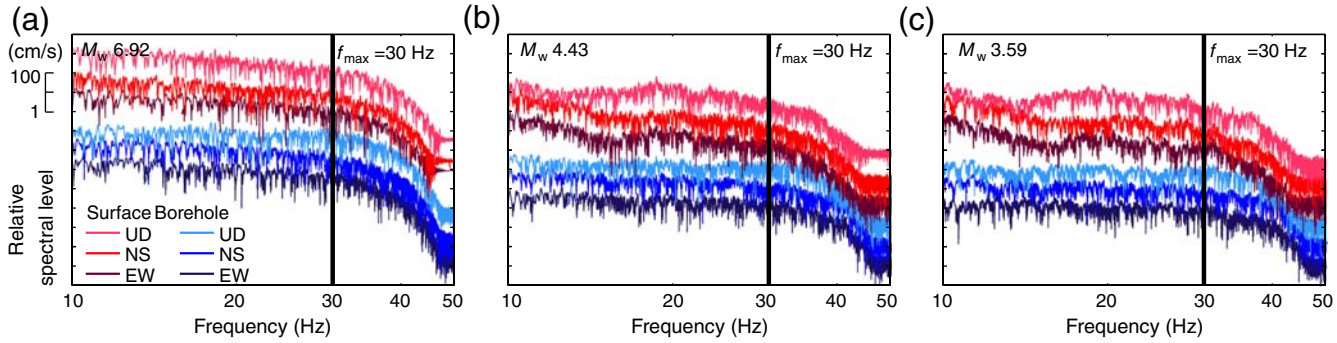

Figure 3. Detail of spectra shown in Figure 2 (bottom row). For each earthquake, six components are shown (from top to bottom: surface UD, NS, EW; borehole UD, NS, EW) offset vertically for ease of interpretation. Solid vertical line illustrates the choice of $f_{\max} = 30$ Hz; for frequencies greater than $f_{\max}$, the spectra all fall off rapidly. While the borehole records are consistently flat up to $f_{\max}$, we attribute the departure of the surface records to surface amplification rather than a different $f_{\max}$. The color version of this figure is available only in the electronic edition.

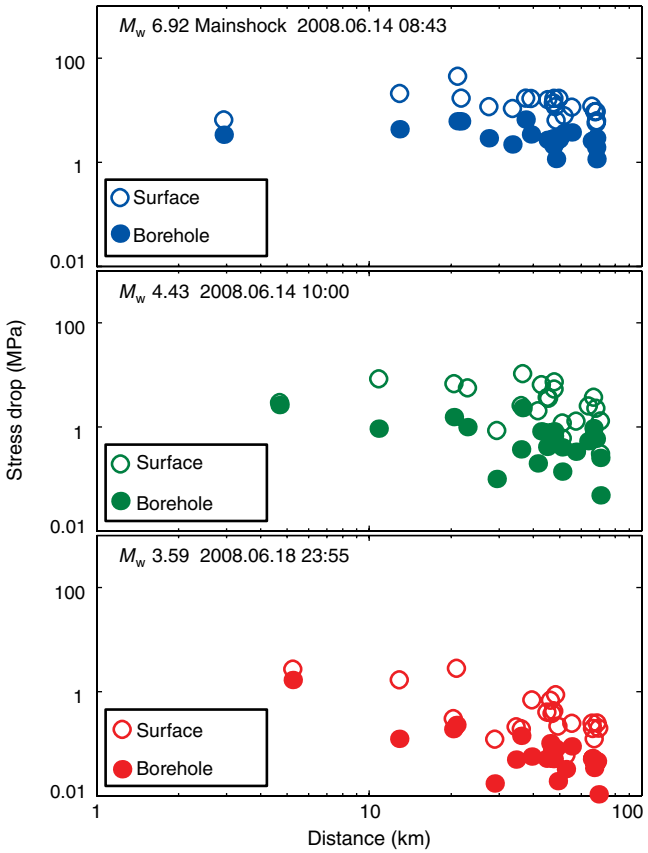

Figure 4. $\Delta\sigma$-a_{rms} as a function of distance for three earthquakes: M_w 6.9 Iwate-Miyagi mainshock; M_w 4.4 Iwate-Miyagi aftershock; and M_w 3.6 Iwate-Miyagi aftershock. $\Delta\sigma$-a_{rms} estimates shown from both surface and borehole data. Surface data are a factor of ~4.5 times as large as borehole data, attributable to surface amplification and differences in seismic impedence. For the mainshock, data are not as affected by attenuation due to their lower f_c and hence wider bandwidth, and the stress-drop estimate is fairly constant with distance. For the smaller aftershocks, however, signal is highly attenuated due to the relatively greater importance of higher frequencies, and stress-drop estimates are much lower at stations farther than ~30 km. The color version of this figure is available only in the electronic edition.

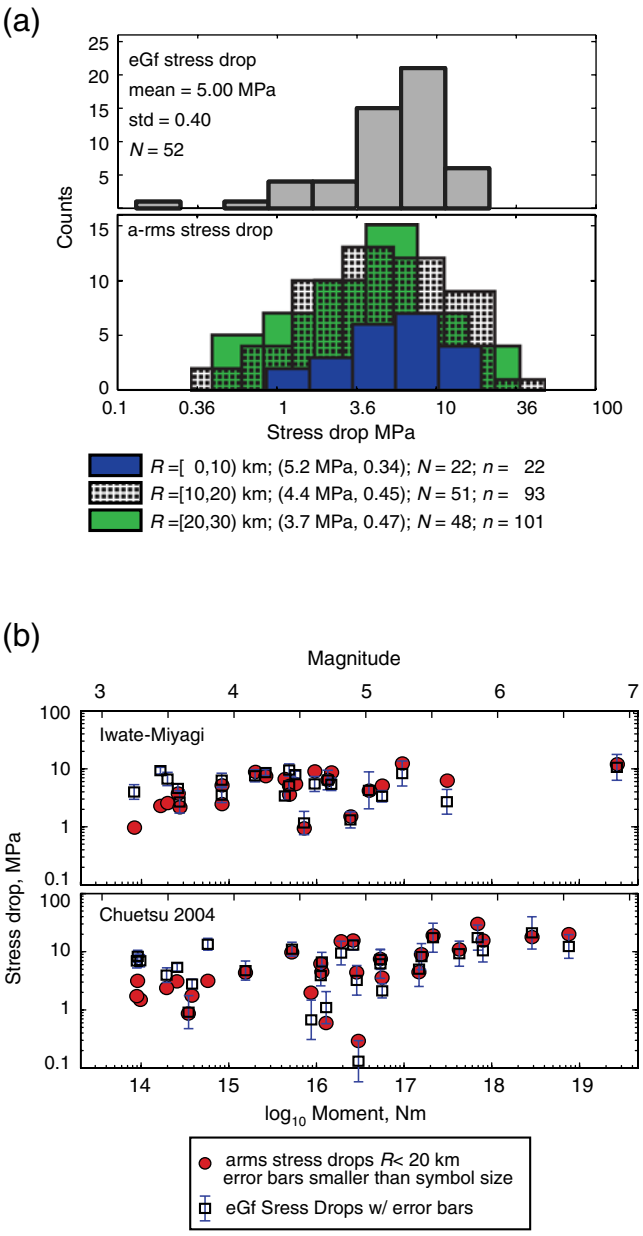

Figure 5. (a) Comparison of log $\Delta\sigma$-eGf distribution with log $\Delta\sigma$-a_{rms} for the Iwate-Miyagi earthquake sequence, with equivalent median and standard deviation given in parentheses, representing the distribution and variability of the overall population of earthquakes. Three different distance ranges are shown: $R < 10$ km, R from 10 to 20 km, and R from 20 to 30 km. As the distance range increases, measurements that are more attenuated are included in the distribution, causing the mean to decrease and the standard deviation to increase. Using only stations within 10 km yields a distribution similar to that for the eGf method. In each case, N is the total number of events considered and shown in the histograms; while n indicates the number of recordings incorporated in total. (b) $\Delta\sigma$-a_{rms} compared to $\Delta\sigma$-eGf, showing the direct comparison of stress drops of each earthquake, and the uncertainty associated with each estimate. Error bars for $\Delta\sigma$-eGf are 95% confidence fit on f_c in $\log_{10}$ units, propagated to $\Delta\sigma$-eGf; error bars for $\Delta\sigma$-a_{rms} are smaller than the symbol size, when error is considered to be from f_c estimates. For most events, the $\Delta\sigma$-a_{rms} is very close to the $\Delta\sigma$-eGf. The color version of this figure is available only in the electronic edition.

rms acceleration is proportionally more strongly attenuated at distance than for larger earthquakes. The $\Delta\sigma$-a_{rms} from all 52 earthquakes as measured at stations within 10 km, from 10–20 km and 20–30 km (Fig. 5a; see Ⓔ Table S1 in the electronic supplement) highlights the loss of bandwidth to attenuation. At $R < 10$ km, the log $\Delta\sigma$-a_{rms} has an equivalent median of 5.2 MPa, and standard deviation of 0.34 ($\log_{10}$ units). With R from 10 to 20 km, the equivalent median decreases to 4.4 MPa due to inclusion of attenuated measurements, and the standard deviation increases to 0.45. At R between 20 and 30 km, the effect of attenuation is more severe, with an equivalent median stress-drop estimate of only 3.7 MPa and standard deviation of 0.47.

In an attempt to account for the attenuation, we compared an ideal, Brune acceleration spectrum that is flat in the frequencies of interest, (f_c, f_{max}), to a modeled attenuated

acceleration spectrum. The attenuated spectrum was modeled with a regionally defined frequency-dependent attenuation of $Q = 64f^{0.8}$ for the highly attenuating region of Eastern Honshu, Japan (Nakamura, 2010). These regionally defined Q models for Japan are strongly frequency-dependent and are valid for small areas. For our study, for any given source-path area, the Q model may be different. Because we are using high frequencies up to 30 Hz (f_{max}), the corrected spectrum becomes unstable and the size of the correction becomes much larger than the original spectrum. Second, we created a loss ratio to represent the percentage of the energy measured as compared to the idealized attenuated spectrum. In both cases, we found that the correction factor was much larger than 50% for most of the recordings, so that the correction was much larger than the measurement. Thus, we choose not to make the correction, and instead to restrict our stress-drop comparison to source-station distances of ≤20 km for which attenuation effects are small. In principle, correction for attenuation effects would allow for further, more distant stations to be used to determine $\Delta\sigma$-a_{rms}.

a_{rms}-Stress Drop Compared to eGf-Stress Drop

We compare the $\Delta\sigma$-a_{rms} to the $\Delta\sigma$-eGf of Baltay *et al.* (2011) in Figures 5 and 6, using source-receiver distances of less than 20 km for the $\Delta\sigma$-a_{rms}. For each sequence, the stress drop is shown for both methods as a function of moment. In most cases the $\Delta\sigma$-a_{rms} compares well to the $\Delta\sigma$-eGf (Fig. 5b). For some of the smaller events, the $\Delta\sigma$-a_{rms} underestimates the $\Delta\sigma$-eGf, due to the increased effect of attenuation acting on the narrower bandwidths of the smaller earthquakes, which have proportionally more high-frequency radiation. The error bars shown for $\Delta\sigma$-eGf are 95% confidence intervals on the f_c fit, in log space, which are propagated to stress-drop errors, ε, so that $\varepsilon(\Delta\sigma\text{-eGf}) = 3^{*}\varepsilon(f_c)$. For $\Delta\sigma$-a_{rms} of individual events, this same propagated error is six times smaller, $\varepsilon(\Delta\sigma\text{-}a_{rms}) = \frac{1}{2}\varepsilon(f_c)$, simply due to the dependence on $f_c^{1/2}$, rather than f_c^3 (Fig. 5b; note: the error bars are not explicitly shown for $\Delta\sigma$-a_{rms} as they are smaller than the symbol size).

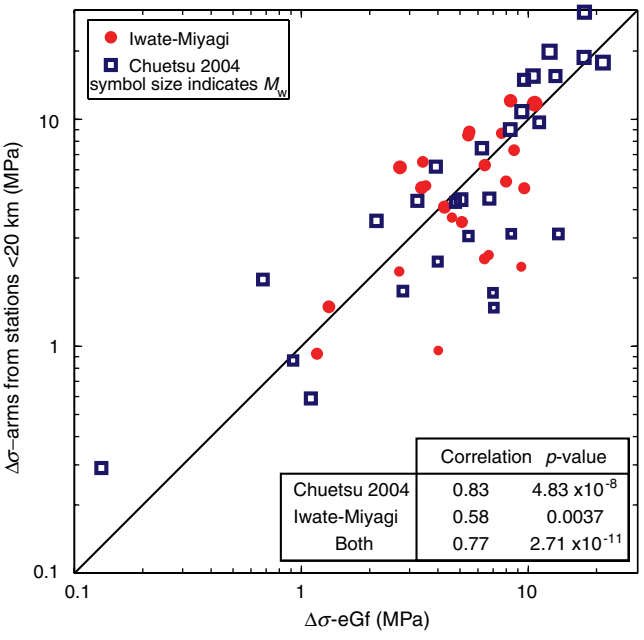

Figure 6. $\Delta\sigma$-a_{rms}, given as the average over all stations within 20 km, compared to $\Delta\sigma$-eGf. The correlation between stress drops is strong for the Chuetsu and Iwate-Miyagi data separately, as well as together. In all cases, the p-value is much less than 0.05, the level of the test indicating that the correlation is significant. Note that the $\Delta\sigma$-a_{rms} recovers a similarly low stress drop, as compared to the $\Delta\sigma$-eGf, for the enervated earthquake in the lower left. The color version of this figure is available only in the electronic edition.

The correlation between log $\Delta\sigma$-a_{rms} and log $\Delta\sigma$-eGf is 0.77 for both sequences considered together, 0.83 for the Chuetsu 2004 sequence alone, and 0.58 for the Iwate-Miyagi sequence. The p-values, or probability of obtaining the above correlation values under the null hypothesis that the two sequences are uncorrelated, are 2.71×10^{-11}, 4.83×10^{-8}, and 0.0037 respectively, much below the 0.05 significance level (95% confidence) of the test, substantiating the significance of the correlations (Fig. 6). One event, highlighted in Baltay *et al.* (2011) with an anomalously low $\Delta\sigma$-eGf, has a similarly low $\Delta\sigma$-a_{rms}, located in the lower left corner of Figure 6.

The $\log_{10}$ $\Delta\sigma$-a_{rms} of the population of earthquakes follows a normal distribution with an equivalent median of 4.4 MPa and standard deviation of 0.42 (for $R < 20$ km), while the $\log_{10}$ $\Delta\sigma$-eGf for the same 52 events also follows a normal distribution, with a very similar median of 5.0 MPa and standard deviation of 0.40 (Fig. 5a). The fact that the overall variation of stress drop is not greatly reduced with the a_{rms} estimates, as was initially expected, indicates that the source of variability in stress-drop measurements reflects inter-event source variability, rather than uncertainty in corner frequency nor inherent uncertainty in either of the two methods considered here.

The comparison of $\Delta\sigma$-a_{rms} with $\Delta\sigma$-eGf illustrates that the eGf method of Baltay *et al.* (2011) effectively removes path and site effects. For close stations ($R < 20$ km) or for larger events for which attenuation at high frequencies has less impact on the a_{rms} measurement, the $\Delta\sigma$-a_{rms} are similar to $\Delta\sigma$-eGf, at a fraction of the computational cost. The eGf method requires a mainshock and a well recorded eGf event at the same station, utilizing assumptions about the corner frequency, spectral shape of the eGf, and an iterative spectral correction scheme (see Baltay *et al.*, 2010). In comparison, the $\Delta\sigma$-a_{rms} is computationally and algorithmically simple, and each event record can be measured independently with fewer assumptions.

For example, the eGf method of estimating $\Delta\sigma$ requires assumptions about spectral shape, taken in Baltay *et al.* (2011) to be the Brune ω^{-2} model, and in turn, assumes an input stress drop to determine the corner frequency of the eGf event. Different choices for starting stress drop affect the final median $\Delta\sigma$-eGf values. Secondly, the determinations

of $\Delta\sigma$-eGf are dependent on the other earthquakes in the sequence in the iterative eGf deconvolution scheme. Baltay (2011) showed that different eGf events can affect the apparent stress by about a factor of 2, for teleseismic eGf deconvolution; assuming error in stress drop is similar to error in apparent stress, the choice of eGf event imposes a stress-drop standard deviation of ~0.15 ($\log_{10}$ units), less than the 0.4 found for the population of $\Delta\sigma$-eGf.

a_{rms} and PGA

PGA or $a_{\max}$ denotes the maximum acceleration recorded in an acceleration time history of an earthquake. It is an important parameter for describing earthquake hazard as it relates directly to the forces imparted upon a structure and can be read directly from a strong-motion seismogram. Though other, more sophisticated, measures of ground motion are currently used in earthquake engineering, PGA is applicable to describe hazard for stiff, high-frequency structures such as nuclear power plants.

While PGA can occur anywhere in the acceleration time history, it almost always occurs in $0 \le t \le T_d$, where 0 denotes the *S*-wave arrival; this window is almost always the window of strongest shaking. Assuming that acceleration time histories in $0 \le t \le T_d$ are stationary, bandlimited, Gaussian white noise, PGA and a_{rms} can be related as

$$\frac{\mathrm{PGA}}{a_{\mathrm{rms}}} = \sqrt{2\ln\left(\frac{2T_d}{T_o}\right)}, \tag{3}$$

where T_d is the duration of the signal, defined above as $1/f_c$, and T_o is the predominant period, taken here to be $1/f_{\max}$, the highest frequency considered (Vanmarcke and Lai, 1977; Hanks and McGuire, 1981). While the exact relationship between T_o and $f_{\max}$ varies somewhat from this assumption (D. Boore, personal comm., 2012), we use the relationship originally implemented by Hanks and McGuire (1981) for consistency with the original analysis. Equation (3) then becomes

$$\frac{\mathrm{PGA}}{a_{\mathrm{rms}}} = \sqrt{2\ln\left(\frac{2f_{\max}}{f_c}\right)}. \tag{4}$$

We measure PGA from the horizontally averaged KiK-net acceleration data, and normalize by the right side of equation (4) to compare to measured a_{rms} (Fig. 7). Both surface and borehole recordings show that PGA is predictable from a_{rms}. The surface recordings are about a factor of 4 larger, attributable to surface amplification and material contrast, as discussed above for $\Delta\sigma$-a_{rms}.

We represent PGA theoretically by combining equations (1) and (4):

$$\mathrm{PGA} = 2R_{\theta\phi}(2\pi)^2 \frac{\Delta\sigma}{106\rho R}\sqrt{\frac{f_{\max}}{f_c}}\sqrt{2\ln\left(\frac{2f_{\max}}{f_c}\right)}, \tag{5}$$

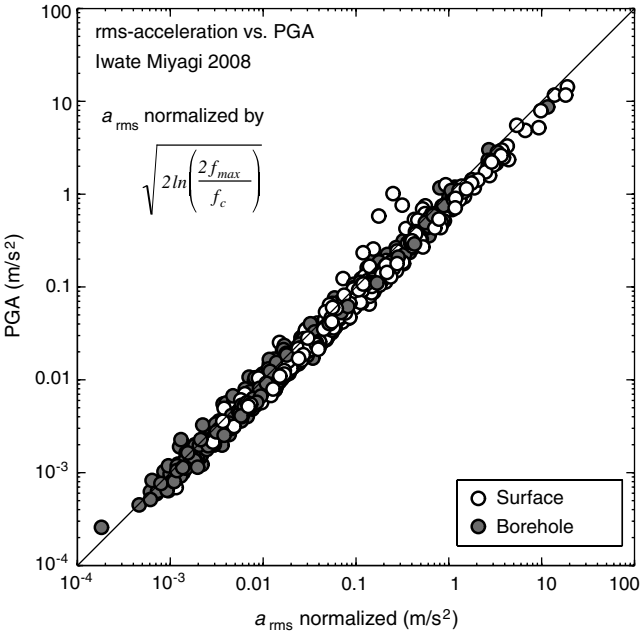

Figure 7. Measured PGA compared to measured rms-acceleration. After normalization, PGA is predictable from rms-acceleration, assuming the relationship derived using random vibration theory. This supports the assumption that acceleration time histories are white, Gaussian noise in the frequency band of interest, and implies that we can use simple stress-drop relations to predict PGA.

and note that it is dependent on stress drop, $\Delta\sigma$, and corner frequency, f_c, for any given earthquake with moment M_0 at distance R. We normalize the PGA to a distance of 10 km, using $1/R$ geometrical spreading. Figure 8 compares the theoretical PGA at a distance of 10 km to the data-measured PGA. While, at first glance, the trends in Figure 8 may not be obvious, we note that the relationship of equation (4), shown as a solid black line, does not account for any attenuation other than simple geometrical spreading. Smaller events, $\sim M_{\mathrm{w}} < 5$, at the farther distances, are proportionally more attenuated due to their narrower bandwidth, and hence the relationship for PGA overestimates those data. Larger earthquakes, and closer recordings, are much better represented by the theoretical PGA.

To model the theoretical PGA, we use an input log stress-drop distribution from Baltay *et al.* (2011) with an equivalent median of 5.12 MPa and standard deviation of 0.42 for the two mainshock-aftershock sequences studied here. The propagated standard deviation for log PGA is 0.51 (dashed lines in Fig. 8). Then for a range of given moments for M_{w} 3–8, we calculate the corner frequency from equation (2), and input the mean stress drop and corner frequency into equation (4).

Substituting in equation (A7) to show PGA as a function of moment, similar to equation (12) of Hanks and McGuire (1981) results in

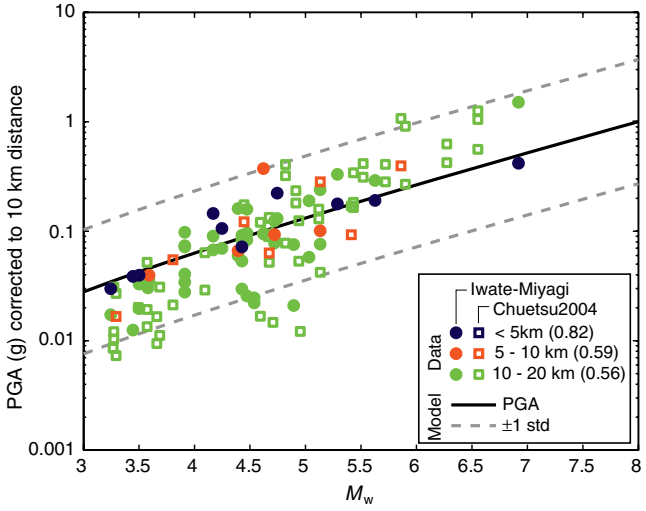

Figure 8. Observed PGA compared to theory-predicted PGA. Solid black line shows the theoretical PGA relation at a 10 km distance. Dashed lines show theoretical PGA ±1 standard deviation, based on the input stress-drop distribution. Measured PGA shown grouped by distance, corrected by $1/R$ geometrical spreading to 10 km. For larger events and closer event-site distances, the theoretical relation does a good job of predicting the data. For smaller events and farther distances, attenuation causes the measured PGA to be much lower than the theoretical predicted PGA, which only assumes a simple $1/R$ geometrical spreading model. The coefficient of determination values for goodness of fit (R^2 value) for each data distance range are given in parentheses; this coefficient is significantly higher for the very close recordings (< 5 km) than it is for farther distances. The color version of this figure is available only in the electronic edition.

$$\mathrm{PGA} \propto \frac{\Delta\sigma^{5/6}}{\rho R \beta^{1/2}} \sqrt{f_{\max}} M_0^{1/6} \sqrt{2 \ln\left(\frac{f_{\max} M_0^{1/3}}{\beta \Delta\sigma^{1/3}}\right)}. \quad (6)$$

This can be approximated as $\mathrm{PGA} \propto M_0^{1/5}$ for $3.0 < M_w < 6.5$. Substituting $\log_{10} M_0 = 1.5\ M_w + 9.05$, we see that the dependence of PGA on magnitude is very weak

$$\log_{10} \mathrm{PGA} \propto 0.3 M_w \quad (7)$$

(Hanks and McGuire, 1981, equation 14). Figure 8 illustrates this trend. Over a factor of a 10^6 in seismic moment, from M_w 3.0 to M_w 7.0, the measured PGA increases by only a factor of ~100, from ~0.01 g to ~1 g. The closest data, within 5 km, which are best represented by the simple model, increase only by a factor of 10 from ~0.03 g at M_w 3.3 to ~0.4 g at M_w 6.9.

For larger events, $M_w > 5.5$, and close stations, $R < 20$ km, the theoretical relationship for PGA fits the data very well. Figure 8 shows the coefficient of determination goodness of fit (R^2 values) of the PGA data to the model (solid black line). For data recorded at < 5 km distance, the model does an excellent job of predicting the data, with a coefficient of determination of 0.82. For the data at greater distances, however, the success of the model fit to the data is decreased, to 0.59 at 5–10 km and to 0.56 at 10–20 km. Although anelastic attenuation has a constant effect on the high-frequency end of the acceleration spectrum for all event sizes at a given distance, smaller earthquakes have a smaller theoretical bandwidth due to their higher corner frequency. Hence, attenuation affects a proportionally greater share of the spectral bandwidth of the smaller events, causing an observed decrease in PGA as compared to the theoretical relationship. Attenuation is greater at the farther distances, and so the affect on smaller events is enhanced. The theoretical formulation for PGA does not model any attenuation or other loss as the waves propagate, and is thus unable to match the data at distances where the amplitudes are significantly decreased by attenuation.

Overall, our results indicate that the theoretical relationships developed can be used to predict PGA reliably for large ($M_w > 5.5$) events at event-station distances up to 30 km, and for $M_w > 3.0$ earthquakes at stations up to ~20 km distance. The loss of energy from attenuation for smaller events and those farther than ~20 km emphasizes the need to develop attenuation relations for describing PGA.

Discussion and Conclusions

We estimate stress drop directly from acceleration records for two earthquake sequences in eastern Honshu, Japan, using seismic moments and corner frequencies determined by Baltay *et al.* (2011). The $\Delta\sigma$-a_{rms} had previously not been rigorously compared to other stress-drop methods using such a well-recorded data set. The $\log_{10} \Delta\sigma$-a_{rms} is normally distributed with an equivalent median of 4.4 MPa and standard deviation of 0.42 ($\log_{10}$ units), comparing well to the $\log_{10} \Delta\sigma$-eGf of Baltay *et al.* (2011), which has an equivalent median of 5.0 MPa and standard deviation of 0.40. However, the $\Delta\sigma$-a_{rms} suffers a loss of signal for smaller events and farther distances due to anelastic attenuation. In this study, we do not correct the time-domain, a_{rms} measurements for any attenuation or other path effect, except a simple $1/R$ spreading correction. Based on corner frequency uncertainty only, the $\Delta\sigma$-a_{rms} yields smaller errors for individual earthquakes. Overall, however, the population of $\Delta\sigma$-a_{rms} shows a similar median and standard deviation to that of the eGf method. These two methods are measuring inherently different parts of the spectrum: frequencies near f_c and below are important in determining the $\Delta\sigma$-eGf, while frequencies higher than the corner are used in the $\Delta\sigma$-a_{rms}, yet both estimate similar stress drops. Our results suggest that the observed standard deviation in stress-drop measurements, approximately 0.4 in $\log_{10}$ units, or a multiplicative factor of 2.5, stems from inter-event source variability, rather than uncertainties in the measurement methods. This also underscores that the eGf method is an improvement over traditional methods of estimating source parameters.

We also use theoretical relationships to predict PGA, and find that for the larger events ($M_w > 5.5$) at distances up to 30 km, and for smaller events at closer distances, < ~10 km, PGA is predictable given a generic input stress-drop distribution and earthquake moment. The variability of a_{rms} from this

data set is similar to that of PGA, not greatly reduced as might be thought (Fig. 7), a result also found by McCann and Boore (1983). While the ability to predict PGA given magnitude and distance is not new, and has been extensively used for ground-motion prediction, the fact that this simple model, with few assumptions, fits the data so well is a testament to the inherent simplicity in the excitation of high-frequency, strong ground motion, measured as PGA.

Our results support the analysis originally performed by Hanks (1979) and Hanks and McGuire (1981), which showed that stress drop could be computed from acceleration records, and that PGA was predictable within 50% from source parameters, for the 16 earthquakes considered in the original study. The underlying assumption that earthquake acceleration records are white Gaussian noise, with a flat power spectral density within the band limit from the corner frequency to the maximum frequency, is reinforced by our results. Furthermore, the $\Delta\sigma$-a_{rms} results further support a self-similar ω^{-2} earthquake model, as discussed in Baltay *et al.* (2011), in that we see no systematic variation in stress drop, however measured, with earthquake size.

Variability in stress drop, both $\Delta\sigma$-eGf and $\Delta\sigma$-a_{rms} as discussed here, is akin to the natural, random, aleatory variability in ground-motion prediction equations, τ, often referred to as expressed as "between event" variability (Al Atik *et al.*, 2010). The variability found in this study from $\Delta\sigma$-eGf and $\Delta\sigma$-a_{rms}, at close distances, is consistent with that of other global source studies (Kanamori and Anderson, 1975; Hanks, 1977; Andrews, 1986; Oth *et al.*, 2010), and in fact is about as low as has been found for any population of earthquakes (e.g., Thatcher and Hanks, 1973, with $\log_{10}$ standard deviation of 0.67; Allmann and Shearer, 2009, $\log_{10}$ stardard deviation of 0.62). Hence, the variability of $\Delta\sigma$-eGf and $\Delta\sigma$-a_{rms} can be used as a bound on the aleatory variability, τ, in ground-motion prediction equations. Stress drop is also an important input parameter to the stochastic method of generating simulated ground motions, so understanding its distribution and variance is central for describing the variability of the output ground motion. Furthermore, as the simple relationships for a_{rms} and PGA employed here (equations A8 and 5) match the strong-motion earthquake data quite well, these source-physics based formulations can be used to understand and model ground-motion data, in order to explore and explain the underlying simplicity in the empirical attenuation relations.

The comparison between the eGf method and $\Delta\sigma$-a_{rms} also emphasizes the robustness of the eGf approach for estimating source parameters, as it accounts for all common source and path effects in the analysis. In the eGf analysis, more data can be incorporated from stations at much farther distances. In order to estimate source parameters with a method that does not rely on direct comparison of events with similar paths, accurate attenuation relations are necessary when incorporating data at distances farther than ~20 km, in high attenuation regions, such as Japan or the Western United States. In tectonic regions that are much less attenuating, such as the Central and Eastern United States (CEUS), or Switzerland, the $\Delta\sigma$-a_{rms} calculation may be possible at much larger distances without accounting for attenuation.

Because of the computational simplicity of $\Delta\sigma$-a_{rms}, it could be estimated in near-real time, as it requires only records from nearby stations and window length T_d (although a_{rms} is not highly dependent on T_d), and some knowledge of the moment, corner frequency, or duration of the event. Such an approach would only require low-intensity data retrieval, and ought to be straightforward to implement. Earthquakes with higher stress drop give rise to larger ground motions, so rapid assessment of earthquake stress drops could provide more reliable ground-motion predictions in the immediate aftermath of an earthquake. $\Delta\sigma$-a_{rms} could also be used in regions where earthquake activity is lower and calibration events that can serve as eGfs are lacking. The fact that these same seismically less active regions are often also less attenuating, as is the case with the CEUS, further recommends adopting $\Delta\sigma$-a_{rms} for this purpose. Finally, $\Delta\sigma$-a_{rms} can be used to expand the current data set of stress-drop measurements, increasing our knowledge of earthquake source parameters and associated aleatory variability.

Data and Resources

Acceleration data from KiK-net database are available online (www.kik.bosai.go.jp/kik/) through the National Research Institute for Earth Science and Disaster Prevention.

Acknowledgments

The authors thank David Boore, Art McGarr, Ralph Archuleta, and an anonymous reviewer, whose thorough comments greatly improved the manuscript. This research was supported by the Southern California Earthquake Center (SCEC). SCEC is funded by NSF Cooperative Agreement EAR-0106924 and USGS Cooperative Agreement 02HQAG0008. The SCEC contribution number for this paper is 1519. A. Baltay was partially supported at Stanford by a Gabilan Stanford Graduate Fellowship, as well as through financial support from Pacific Gas and Electric.

References

Aki, K. (1967). Scaling law of seismic spectrum, *J. Geophys. Res.* **72,** 1217–1231.

Al Atik, L., N. Abrahamson, J. J. Bommer, F. Scherbaum, F. Cotton, and N. Kuehn (2010). The variability of ground-motion prediction models and its components, *Seismol. Res. Lett.* **81,** no. 5, 794–801.

Allmann, B. P., and P. M. Shearer (2009). Global variations of stress drop for moderate to large earthquakes, *J. Geophys. Res.* **114,** B01310, doi: 10.1029/2008JB005821.

Anderson, J. G. (1986). Implications of attenuation for studies of the earthquake source, in *Earthquake Source Mechanics*, S. Das, J. Boatwright, and C. H. Scholz (Editors), AGU Monograph **37**, 311–318.

Anderson, J. G., and S. E. Hough (1984). A model for the shape of the Fourier amplitude spectrum of acceleration at high frequencies, *Bull. Seismol. Soc. Am.* **74,** no. 5, 1969–1993.

Andrews, D. J. (1986). Objective determination of source parameters and similarity of earthquakes of different size, in *Earthquake Source*

Mechanics, S. Das, J. Boatwright, and C. H. Scholz (Editors), AGU Monograph, **37,** 259–267.

Archuleta, R. J., E. Cranswick, C. Mueller, and P. Spudich (1982). Source parameters of the 1980 Mammoth Lakes, California, earthquake sequence, *J. Geophys. Res.* **87,** 4595–4607.

Atkinson, G. M., and D. M. Boore (2006). Earthquake ground-motion prediction equations for eastern North America, *Bull. Seismol. Soc. Am.* **96,** no. 6, 2181–2205, doi: 10.1785/0120050245.

Baltay, A., S. Ide, G. Prieto, and G. Beroza (2011). Variability in earthquake stress drop and apparent stress, *Geophys. Res. Lett.* **38,** L06303, doi: 10.1029/2011GL046698.

Baltay, A., G. Prieto, and G. C. Beroza (2010). Radiated seismic energy from coda measurements and no scaling in apparent stress with seismic moment, *J. Geophys. Res.* **115,** B08314.

Baltay, A. S. (2011). Precise Earthquake Source Parameter Estimation, *Ph.D. Thesis*, Stanford University, Stanford, California.

Boore, D. M. (1983). Stochastic simulation of high-frequency ground motions based on seismological models of the radiated spectra, *Bull. Seismol. Soc. Am.* **73,** 1865–1894.

Boore, D. M. (2003). Simulation of ground motion using the stochastic method, *Pure Appl. Geophys.* **160,** 635–676.

Boore, D. M. (2012). Updated determination of stress parameters for several well-recorded earthquakes in Eastern North America, *Seismol. Res. Lett.* **83,** 190–199.

Boore, D. M., K. W. Campbell, and G. M. Atkinson (2010). Determination of stress parameters for eight well-recorded earthquakes in eastern North America, *Bull. Seismol. Soc. Am.* **100,** 1632–1645.

Boore, D. M., E. M. Thompson, and H. Cadet (2011). Regional correlations of V_{S30} and velocities averaged over depths less than and greater than 30 m, *Bull. Seismol. Soc. Am.* **101,** no. 6, 3046–3059.

Brune, J. N. (1970). Tectonic stress and the spectra of seismic shear waves from earthquakes, *J. Geophys. Res.* **75,** no. 26, 4997–5009.

Bycroft, G. N. (1960). White noise representation of earthquakes, *J. Eng. Mech. Div., ACSE* **86,** no. 2, 1–16.

Hanks, T. C. (1977). Earthquake stress drops, ambient tectonic stresses and stresses that drive plate motions, *Pure Appl. Geophys.* **115,** 441–458.

Hanks, T. C. (1979). b-values and ω-γ seismic source models: Implications for tectonic stress variations along active crustal fault zones and the estimation of high-frequency strong ground motion, *J. Geophys. Res.* **84,** 2235–2242.

Hanks, T. C. (1982). fmax, *Bull. Seismol. Soc. Am.* **72,** 1867–1879.

Hanks, T. C., and R. K. McGuire (1981). The character of high-frequency strong ground motion, *Bull. Seismol. Soc. Am.* **71,** 2071–2095.

Hanks, T. C., and W. Thatcher (1972). A graphical representation of seismic source parameters, *J. Geophys. Res.* **77,** 4292–4405.

Hikima, K., and K. Koketsu (2005). Rupture processes of the 2004 Chuetsu (mid-Niigata prefecture) earthquake, Japan: A series of events in a complex fault system, *Geophys. Res. Lett.* **32,** L18303, doi: 10.1029/2005GL023588.

Housner, G. (1947). Characteristics of strong-motion earthquakes, *Bull. Seismol. Soc. Am.* **37,** 19–31.

Kanamori, H., and D. Anderson (1975). Theoretical basis for some empirical laws of seismology, *Bull. Seismol. Soc. Am.* **65,** 1073–1095.

Kane, D. L., G. A. Prieto, F. L. Vernon, and P. M. Shearer (2011). Quantifying seismic source parameter uncertainties, *Bull. Seismol. Soc. Am.* **101,** 535–543.

Margaris, B. N., and D. M. Boore (1998). Determination of $\Delta\sigma$ and $\kappa 0$ from response spectra of large earthquakes in Greece, *Bull. Seismol. Soc. Am.* **88,** 170–182.

McCann, M. W., and D. M. Boore (1983). Variability in ground motions: Root mean square acceleration and peak acceleration for the 1971 San Fernando, California, earthquake, *Bull. Seismol. Soc. Am.* **73,** 615–632.

McGuire, R. K., and T. C. Hanks (1980). rms accelerations and spectral amplitudes of strong ground motion during the San Fernando, California Earthquake, *Bull. Seismol. Soc. Am.* **70,** 1907–1919.

Nakamura, R. (2010). 3-D Attenuation structure beneath the Japanese islands, source parameters and site amplification by simultaneous inversion using short period strong motion records and predicting strong ground motion, *Ph. D. Thesis*, University of Tokyo, Japan.

Oth, A., D. Bindi, S. Parolai, and D. Di Giacomo (2010). Earthquake scaling characteristics and the scale-(in)dependence of seismic energy-to-moment ratio: Insights from KiK-net data in Japan, *Geophys. Res. Lett.* **37,** L19304, doi: 10.1029/2010GL044572.

Oth, A., D. Bindi, S. Parolai, and D. Di Giacomo (2011). Spectral analysis of K-NET and Kik-net data in Japan, Part II: On attenuation characteristics, source spectra, and site response of borehole and surface station, *Bull. Seismol. Soc. Am.* **101,** doi: 10.1785/0120100135.

Papageorgiou, A. S., and K. Aki (1983). A specific barrier model for the quantitative description of inhomogeneous faulting and the prediction of strong ground motion, Part I: Description of the model, *Bull. Seismol. Soc. Am.* **73,** 693–722.

Shearer, P. M., G. A. Prieto, and E. Hauksson (2006). Comprehensive analysis of earthquakes source spectra in southern California, *J. Geophys. Res.* **111,** doi: 10.1029/2005JB003979.

Sonley, E., and R. E. Abercrombie (2006). Effects of methods of attenuation correction on source parameter determination, in *Earthquakes: Radiated Energy and the Physics of Faulting*, Geophys. Monogr. Ser., R. Abercrombie *et al.*, (Editors), Vol. 170, AGU, Washington, DC, 91–97.

Suzuki, W., S. Aoi, and H. Sekiguchi (2010). Rupture process of the 2008 Iwate-Miyagi Nairiku, Japan, earthquake derived from near-source strong-motion records, *Bull. Seismol. Soc. Am.* **100,** no. 1, doi: 10.1785/0120090043.

Thatcher, W., and T. C. Hanks (1973). Source parameters of Southern California earthquakes, *J. Geophys. Res.* **78,** no. 35, 8547–8576, doi: 10.1029/JB078i035p08547.

Vanmarcke, E. H., and S. P. Lai (1977). *Strong-Motion Duration of Earthquakes*, Dept. of Civil Eng. Pub. No. R77-16, Massachusetts Institute of Technology, Cambridge.

Appendix A

Derivation of the a_{rms} Stress Drop

The root mean square (rms) value of an acceleration time history can be related to stress drop (equation 3), corner frequency, and $f_{\max}$. The following derivation (equations A1–A9), given originally in Hanks (1979), is rederived here to refresh the reader. Parseval's Theorem states that the energy in the time domain is equal to the energy in the frequency domain (following Hanks, 1979, equation 10),

$$\int_{-\infty}^{\infty} |a(t)|^2 dt = \frac{1}{2\pi}\int_{-\infty}^{\infty} |\tilde{a}(\omega)|^2 d\omega = \frac{1}{\pi}\int_{0}^{\infty} |\tilde{a}(\omega)|^2 d\omega. \tag{A1}$$

The second equality in equation (A1) arises because the squared function is symmetric. Assuming significant motion is recorded at close stations only for the duration of faulting, and that the signal is bandlimited from f_c to $f_{\max}$, we rewrite (equation A1) as

$$\int_{0}^{T_d} |a(t)|^2 dt = \frac{1}{\pi}\int_{2\pi f_c}^{2\pi f_{\max}} |\tilde{a}(\omega)|^2 d\omega \tag{A2}$$

(Hanks, 1979, equation 11). For spectra following a Brune (1970) model,

$$|\tilde{a}(\omega)| = 2\frac{1}{\sqrt{2}}R_{\theta\phi}\frac{\Omega_o}{(1+(\omega/\omega_c)^2}, \tag{A3}$$

where Ω_o is the long period spectral level, proportional to the moment. The factor of 2 accounts for free surface amplification; the factor of $1/\sqrt{2}$ accounts for partitioning of ground motion primarily onto two horizontal components; and $R_{\theta\phi}$ is the shear-wave radiation pattern. For $f_c \le f \le f_{\max}$ (and hence $\omega_c \le \omega \le \omega_{\max}$)

$$|\tilde{a}(\omega)| = \sqrt{2}R_{\theta\phi}\Omega_o\omega_c^2 = \sqrt{2}R_{\theta\phi}\Omega_o(2\pi f_c)^2 \tag{A4}$$

(Hanks, 1979, equation 13).

The rms of acceleration, a_{rms}, over the interval $[0, T_d]$ is defined as

$$a_{\text{rms}} = \sqrt{\frac{1}{T_d}\int_0^{T_d}|a(t)|^2dt} \tag{A5}$$

(Hanks, 1979, equation 12). Combining equations (A2)–(A5), with $f_{\max} \gg f_c$, so that $f_{\max}$-$f_c \approx f_{\max}$, and assuming $T_d = 1/f_c$,

$$\begin{aligned} a_{\text{rms}} &= \sqrt{\frac{1}{T_d}\frac{2}{2\pi}\int_{2\pi f_c}^{2\pi f_{\max}}|\tilde{a}(\omega)|^2d\omega} \\ &= \sqrt{f_c\frac{1}{\pi}|\sqrt{2}R_{\theta\phi}\Omega_o(2\pi f_c)^2|^2(2\pi f_{\max}-2\pi f_c)} \\ a_{\text{rms}} &= 2R_{\theta\phi}(2\pi)^2\Omega_o f_c^3\sqrt{\frac{f_{\max}}{f_c}}. \end{aligned} \tag{A6}$$

For the Brune ω^{-2} model, stress drop is related to Ω_o as (e.g., Hanks and Thatcher, 1972),

$$\Delta\sigma = 106\rho R\Omega_o f_c^3. \tag{A7}$$

In this study, we take R as the hypocentral distance. For the larger earthquakes, this distance may not be the most applicable, but it is the simplest for our case and indistinguishable from other measures for all but the largest earthquakes in our population. Combining equation (A6) with equation (A7) gives (Hanks, 1979, equation 17)

$$a_{\text{rms}} = 2R_{\theta\phi}(2\pi)^2\frac{\Delta\sigma}{106\rho R}\sqrt{\frac{f_{\max}}{f_c}}. \tag{A8}$$

The stress drop, $\Delta\sigma$-a_{rms}, is then expressed in terms of a_{rms}, $f_{\max}$, and f_c, as in equation (1), where we assume a density $\rho = 2800$ kg/m^3; and $R_{\theta\phi} = 0.6$ is the rms value of shear-wave radiation pattern

$$\Delta\sigma_{a_{\text{rms}}} = a_{\text{rms}}\frac{106\rho R}{2R_{\theta\phi}(2\pi)^2}\sqrt{\frac{f_c}{f_{\max}}}. \tag{A9}$$

Department of Geophysics
Stanford University
397 Panama Mall
Stanford, California 94305
(A.S.B., G.C.B.)

United States Geological Survey
345 Middlefield Road
Menlo Park, California 94025
(T.C.H.)

Manuscript received 1 May 2012